

APPLICATION OF ATTENUATED TOTAL REFLECTANCE-FOURIER TRANSFORM INFRARED SPECTROSCOPY (ATR-FTIR) TO EVALUATE IMPACT OF ROCK HETEROGENEITIES ON HYDROCARBON DISTRIBUTION IN DELTAIC RESERVOIR SANDSTONES

Joel Ben-Awuah^{1*} and Eswaran Padmanabhan²

¹ Department of Petroleum Engineering, Faculty of Engineering, Technology and Built Environment, UCSI University, Jalan Choo Lip Kung, Taman Taynton View, 56000 Cheras, Kuala Lumpur, Malaysia

² Department of Geosciences, Faculty of Geosciences and Petroleum Engineering, Universiti Teknologi PETRONAS, Bander Seri Iskandar, 31750 Tronoh, Perak Darul Ridzuan, Malaysia

Received July 12, 2016; Accepted November 7, 2016

Abstract

Hydrocarbon functional groups distribution have been analyzed on 1*1cm grid on sample surfaces using ATR-FTIR spectroscopy to determine hydrocarbon bond type variation and factors controlling it. Micropermeability measurements have been carried out to determine relationship between absorbance of hydrocarbon functional groups and permeability. The main hydrocarbon functional groups recorded in the samples are the aliphatic C-H and aromatic C=C-C bonds. The aromatic functional groups are more concentrated in the silt-dominated laminations of the laminated sandstones and burrows in the bioturbated sandstones compared to the sand-dominated laminations and non-burrowed zones respectively. Textural, structural and bioturbation induced heterogeneities that influence pore size and permeability distribution in the samples is found to be the main factor controlling distribution of hydrocarbon bonds. In samples that lack any form of macro scale heterogeneities, hydrocarbon and permeability distribution are found to be random. High permeability generally correlates negatively with absorbance of hydrocarbon bonds and vice versa.

Keywords: FTIR spectroscopy; hydrocarbon functional groups; micropermeability; deltaic sandstones; rock heterogeneities; West Baram Delta; Sarawak Basin.

1. Introduction

Deltaic and fluvial reservoirs contain the majority of hydrocarbon reservoirs in the world [1] and show extensive spatial variability in facies distribution and reservoir heterogeneity [2-6]. Reservoir heterogeneity in sandstone bodies occur at various extents and scales, ranging from micrometers to hundreds of meters. These heterogeneities are generally associated with facies distribution, texture, lithology and bioturbation, and often affects reservoir properties and consequently hydrocarbon distribution [7-9].

The impact of reservoir rock heterogeneities on hydrocarbon distribution is well-researched and has evolved significantly over time [10-13]. However, most of these studies have focused on quantifying reservoir heterogeneities and incorporating them in large scale reservoir simulations and modeling to predict hydrocarbon migration patterns. Experimental studies on the connection between rock heterogeneities and hydrocarbon distribution particularly at the macro and micro scales are rare in recent literature [14-15]. The objective of this study is to contribute in bridging this gap in knowledge through the use of ATR-FTIR and micro permeametry to determine the impact of textural, structural and bioturbation-induced heterogeneities on hydrocarbon and permeability distribution. Reservoir sandstones from West Baram Delta in the offshore Sarawak Basin have been used in this study.

Traditionally, spectroscopic methods such as UV-Vis, FTIR and NMR have been used in the evaluation of liquid petroleum yield of hydrocarbon source rocks [16-20] with very little application in the evaluation of hydrocarbon distribution in reservoir rocks. Recent advances in FTIR spectroscopy especially in the development of ATR-FTIR has made it possible for such investigations to be carried out on both liquid and solid samples. The portion of the infrared spectrum practically used in infrared spectroscopy is the limited portion between 4000 and 400 cm^{-1} known as the mid-infrared region [21]. The technique is based on the vibration of the atoms in a molecule and the spectrum obtained depends on what fraction of the incident radiation is absorbed at a particular energy [22]. The molecular fingerprint of a sample is composed of functional groups within the sample that characterize the chemical reactions of molecules within which they are found. The frequency of vibration of a molecule in a sample corresponds to specific peaks in the absorption spectrum. Based on comparisons with thousands of compounds containing various functional groups, chemists have concluded that most functional groups have characteristic infrared absorption bands whose location varies little in the infrared spectra of all compounds that contain that functional group [23]. Hydrocarbons, just like any other molecules, also have characteristic bands that are easily recognizable on the FTIR spectrum making this technique well suited for such studies.

2. Geological Setting

The West Baram Delta is one of seven geological provinces found offshore the Sarawak foreland basin [24] and is the most prolific of all the geological provinces in the basin [25]. The delta is estimated to have more than 400 million stock barrels of oil in place with multiple stacked sandstone reservoirs in a shallow offshore environment and has been in production for the past 30 years. The part of the delta in the Sarawak basin spans an area of 7500 square km with 2500 square km of it onshore [26-27]. A major northeast-trending fault zone known as the West Baram Line forms the western margin of the province and separates the delta from the older and more stable Balingian and Central Luconia Provinces [28]. Sediments supply to the basin is thought to have been derived from the erosion of the uplifted Rajang Fold-Thrust Belt and several phases of tectonism and uplift of the hinterland during the Neogene [29-30]. During Late Cretaceous to Paleocene, the Sarawak margin was the site of southward subduction of a proto-South China Sea oceanic crust [31].

The stratigraphic architecture of the delta was constructed by Middle to Upper Miocene thick and sandy progradational shallow marine-deltaic sequences which are separated by transgressive marine shale intervals [25]. Sediments deposition is characterized by the outbuilding of northward progradational sequences which were initiated in Middle Miocene times [28]. An estimated thickness of about 6000-9000m Neogene clastic sediments of coastal to coastal marine sands and shales make up the stratigraphy of the delta [32]. Eight sedimentary cycles were identified by [26] in the West Baram Delta. The studied samples belong to the Middle to Upper Miocene Cycles V and VI sequences.

3. Materials and Methods

The study involves core samples from 4 wells in 3 offshore oil fields from the West Baram Delta (Figure 1). Sample description was carried out on conventional cores from the wells with emphasis on lithology, texture (grain size, grain sorting and grain shape), structure and bioturbation [6, 33-34]. Conventional core description was complimented with thin section analysis.

An Agilent Technologies Cary 660 Series FTIR Spectrometer equipped with a PIKE MIRACLE diamond attenuated total reflectance spectroscopy (ATR) and mid infrared (MIR=4000-400 cm^{-1}) source has been used. The instrument settings used in this study include 16 sample scans and 4 cm^{-1} resolution and aperture. The limit of detection of the instrument is 0.08%. Background scans were done with the same settings used for the sample analysis and replicate spectra collected on selected samples to check consistency of peak positions and absorbance intensities. Point samples covering the different textural and structural domains within a sample

were taken on a 1*1cm grid drawn on core slabs for analysis. The spectrum obtained is processed and analyzed using the Agilent Resolutions Pro software.

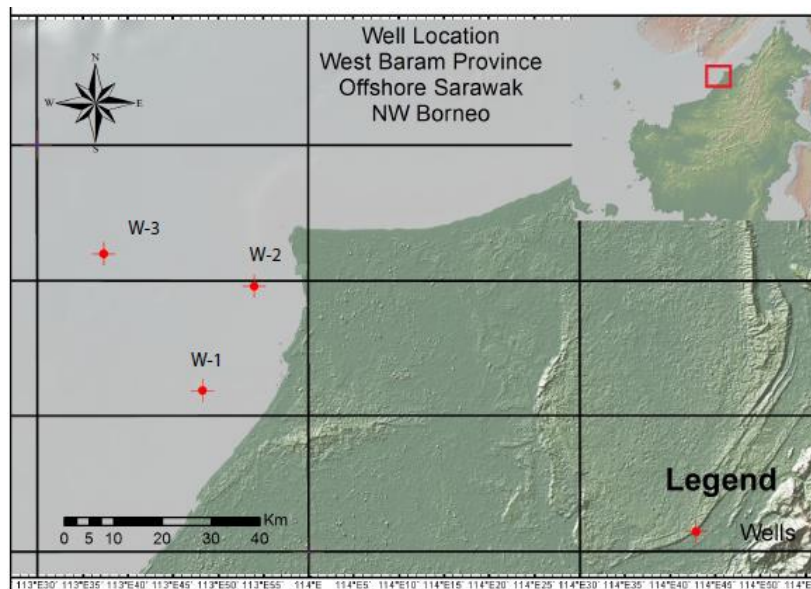


Figure 1. Location map of study area showing studied wells [43]

The tiny perm measurements were carried out at points on the 1*1cm grid at which samples were taken for the FTIR analysis. The measurements were done with an NER Tiny Perm II portable air permeameter. Three to five measurements were taken at each point and the values averaged to get one representative value. The measurements obtained from the Tiny Perm II are cross-referenced with the included calibration curves to obtain absolute permeability in milliDarcies.

A Thermo Scientific PASCAL 240 series mercury porosimeter was used to measure the porosity and pore size distribution in this study according to [35]. A maximum test pressure of 200 MPa, at a temperature of 25 °C and mercury density of 13.53 g/cm³ were used.

Thin sections were made for microscopic analysis of the samples. The thin sections were made according to procedures described by [36]. The friable samples were impregnated with resin to harden them before slicing. Blue dye was added to the resin for easier identification of pores.

4. Results and Discussion

4.1. Samples Description

Three main sandstone types have been identified and analyzed for heterogeneities in hydrocarbon and permeability distribution. These include massive fine grained sandstones, bioturbated sandstones and parallel laminated sandstones.

4.1.1. Massive fine grained sandstones (MFGS)

The massive fine grained sandstones (MFGS) are the dominant sandstone lithofacies in all the wells studied. The MFGS grain sizes vary between very fine to fine and are angular to subangular (Figure 2a) indicating relatively lower levels of depositional energy and shorter transport distance [6, 33]. They are poorly structured, consolidated and slightly to fairly porous. The porosity and permeability values recorded in the MFGS at 95% confidence level range between 18.7-20.9% and 77.9-423.5mD respectively. These samples generally lack any form of macro scale heterogeneities making them appear relatively homogenous.

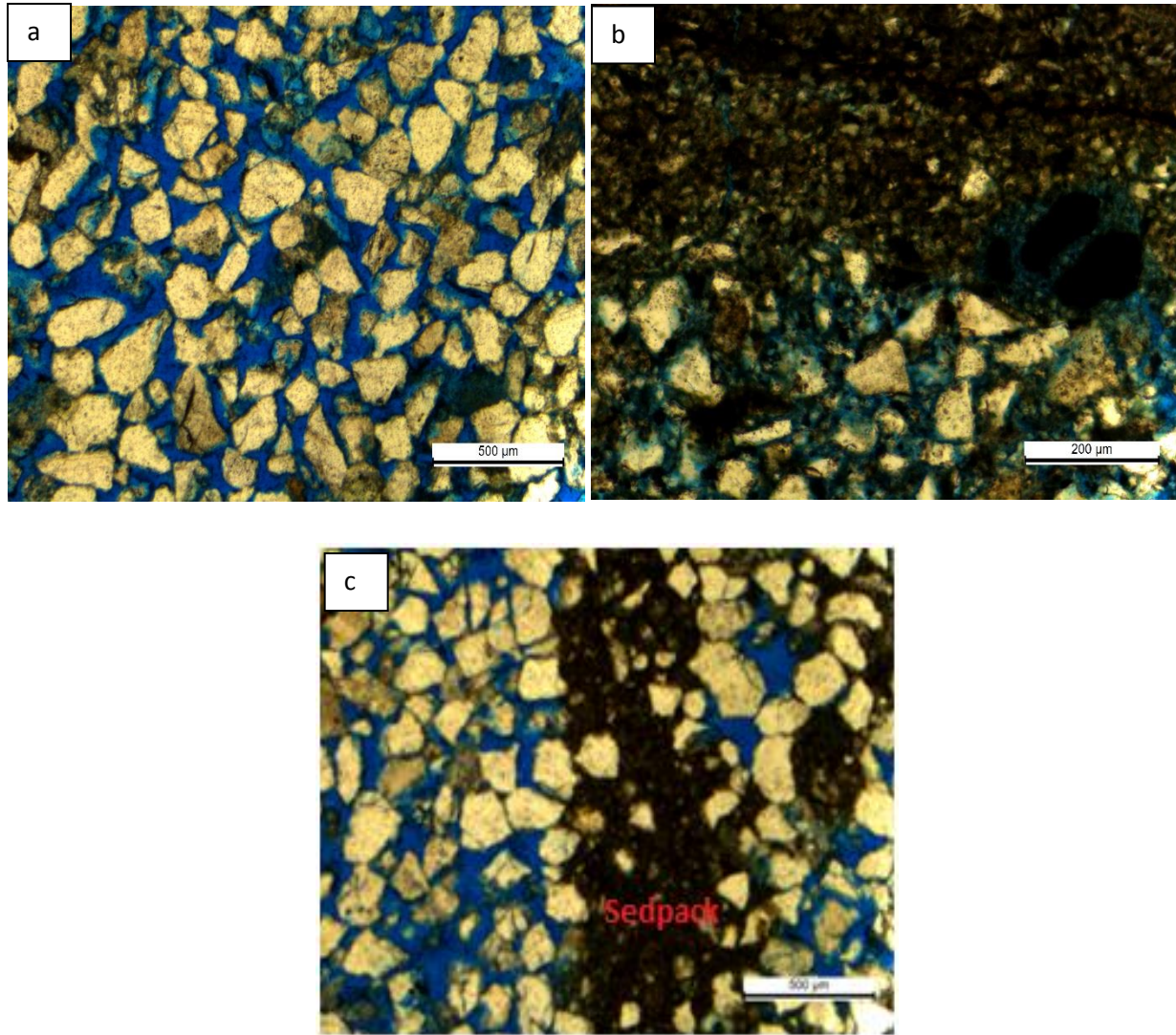


Figure 2. Thin section photomicrographs of (a) massive fine grained sandstone, (b) parallel laminated sandstone and (c) bioturbated sandstone.

4.1.2. Parallel laminated sandstones (PLS)

The PLS are characterized by planar/ parallel horizontal laminations with lamina thickness between 1-3cm. The laminations consist of alternating silt-dominated and sand-dominated laminations (Figure 2c). They are consolidated and fairly porous with poorly sorted angular grains. Laminations in sedimentary rocks generally indicate cyclic changes in the supply of sediments in the basin mainly due to variations (low or high) in the depositional energy [6]. The porosity and permeability values recorded in the PLS at 95% confidence level range between 18.5-21% and 90.8-128.9mD respectively.

4.1.3. Bioturbated sandstone (BS)

The BS are characterized by the presence of abundant burrows from the burrowing activities (sedpack) of bioturbators (Figure 2c). They are poorly structured with grain sizes varying between very fine to medium grained. The grains are angular to subangular in shape with sorting ranging from moderately sorted in the host sandstones and poorly sorted to unsorted in the burrows. Based on the [37] bioturbation index (BI) classification scheme, BI grade

ranging between 3-5 (moderate-intense bioturbation) is assigned to sections of the bioturbated facies depending on the burrow abundance, burrow overlap and sharpness of the primary sedimentary fabric. Porosity and permeability in the bioturbated samples is significantly reduced compared to their non-bioturbated equivalent due to the activities of bioturbators such as the indiscriminate mechanical mixing of sediments and selective concentration of mud and organic matter in burrows and burrow linings [38-40]. Porosity and permeability in the burrows are comparatively lower than the host sandstones. The porosity and permeability values recorded in the BS at 95% confidence level range between 14.5-16.8% and 16.2-28.6mD respectively.

4.2. General spectral features and hydrocarbon peaks analysis

Analysis of the FTIR spectra was limited to the regions of interest which are the hydrocarbon functional group ranges. The main hydrocarbon functional groups in infrared spectra occur between $2800\text{-}3200\text{cm}^{-1}$ for aliphatic functional groups and $1700\text{-}2000\text{cm}^{-1}$, $1430\text{-}1600\text{cm}^{-1}$, $1000\text{-}1275\text{cm}^{-1}$ and $690\text{-}900\text{cm}^{-1}$ for aromatic functional groups [21-22, 41]. The part of the spectrum between 1400 to 625cm^{-1} known as the fingerprint region contains a very complex series of absorption bands and correlations between any of them and specific functional groups are difficult to make [23].

The spectra of the samples generally show distinct bands at 3700 , $2800\text{-}3000$, 1500 , $1030\text{-}1090$, 800 , and $600\text{-}700\text{cm}^{-1}$ (Figure 3). The bands at 3700cm^{-1} and $600\text{-}700\text{cm}^{-1}$ represent O-H peaks and is attributed to the clays and moisture in the samples [22]. The quartz in the samples is represented by Si-O-Si stretching bands between $1030\text{-}1090\text{cm}^{-1}$ and Si-Si stretching bands at 800cm^{-1} . The Si-O-Si peaks are the most dominant in all the samples due to the high quartz content. The bands between $2800\text{-}3000\text{cm}^{-1}$ represent the aliphatic C-H stretching and C-H bending moieties while the peak at 1500cm^{-1} is due to aromatic C=C vibrations [21-22, 41].

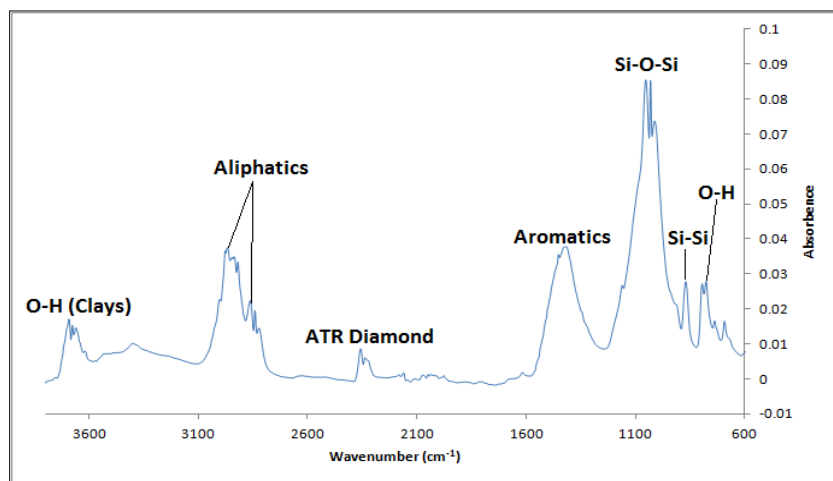


Figure 3. FTIR spectrum showing the main functional groups across the samples.

4.3. Spatial Variations in Hydrocarbon Distribution

4.3.1. Parallel laminated sandstones

The distribution of hydrocarbon bonds in the parallel laminated sandstones is much more complex and varies mainly with the lamination type (Figure 4). The aromatic functional groups are more concentrated in the silt-dominated laminations compared to the sand-dominated laminations which have high aliphatic content. The aliphatic moieties include the C-H stretching bonds while the main aromatic functional group detected is the C=C-C stretching bond. Analysis of the pore size distribution in the parallel laminated sandstones (Table 1) indicates

two main ranges of pore sizes (bimodal pore size distribution) corresponding to the silt-dominated laminations and sand-dominated laminations (Figure 5). The silt-dominated laminations have predominantly micro to meso pores ranging in size between 200-1000 nm whereas the sand-dominated laminations have predominantly lower to upper macro pores with pore sizes ranging between 3000-30000 nm. The concentration of hydrocarbon functional groups in the silt-dominated laminations can therefore be attributed to its smaller pore sizes which makes them able to retain a lot more hydrocarbons compared to the sand-dominated laminations.

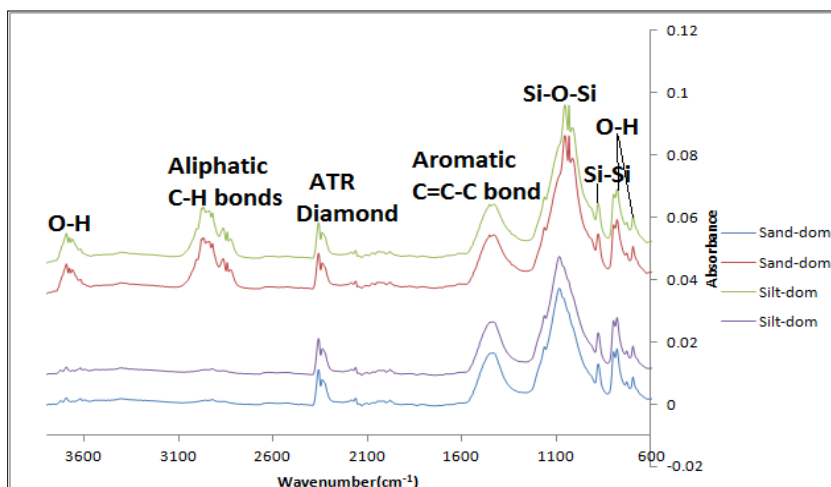


Figure 4. FTIR spectra of parallel laminated sandstones showing dominance of aromatic functional groups in the silt-dominated laminations.

Table 1. Pore size distribution in different sandstone types

Facies	Pore Size(nm)				Pore Type
	Min	Max	Min	Max	
MFGS	4000	20000			Lower to upper macro
PLS	200	1000	3000	30000	Micro to meso ,Lower to upper macro
BS	20	30	700	8000	Nano to micro, Meso to lower macro

4.3.2. Bioturbated sandstones

The bioturbated sandstones are characterized by the presence of burrows of different types, geometry and sizes. The distribution of hydrocarbon functional groups in the bioturbated samples is found to follow the distribution of burrows. The hydrocarbon functional groups are more concentrated in the burrows compared to the host sandstones (Figure 6). The burrows are also relatively richer in aromatic functional groups. The dominance of aromatic functional groups in the burrows compared to the host sandstones can be attributed to pore size variations between the two zones. The smaller pore sizes in the burrows (20-30nm) compared to bigger pore sizes in the host sandstones (700-8000nm) may prevent the larger aromatic functional groups from migrating out of them whereas the smaller aliphatic functional groups can migrate easily out of the burrows regardless of the smaller pore sizes resulting in the selective concentration of aromatic bonds in the burrows.

4.3.3. Massive fine grained sandstone

Compared to the parallel laminated sandstones and bioturbated sandstones, hydrocarbon functional groups distribution in the massive fine-grained sandstones is quite random. Hydrocarbons may be present at one point and completely absent at the next point. At the points where hydrocarbons are present, similar FTIR spectra representing similar bonds are

observed (Figure 7). Aliphatic C-H stretching and aromatic C=C stretching bonds are the main hydrocarbon functional groups detected in the massive fine grained sandstone.

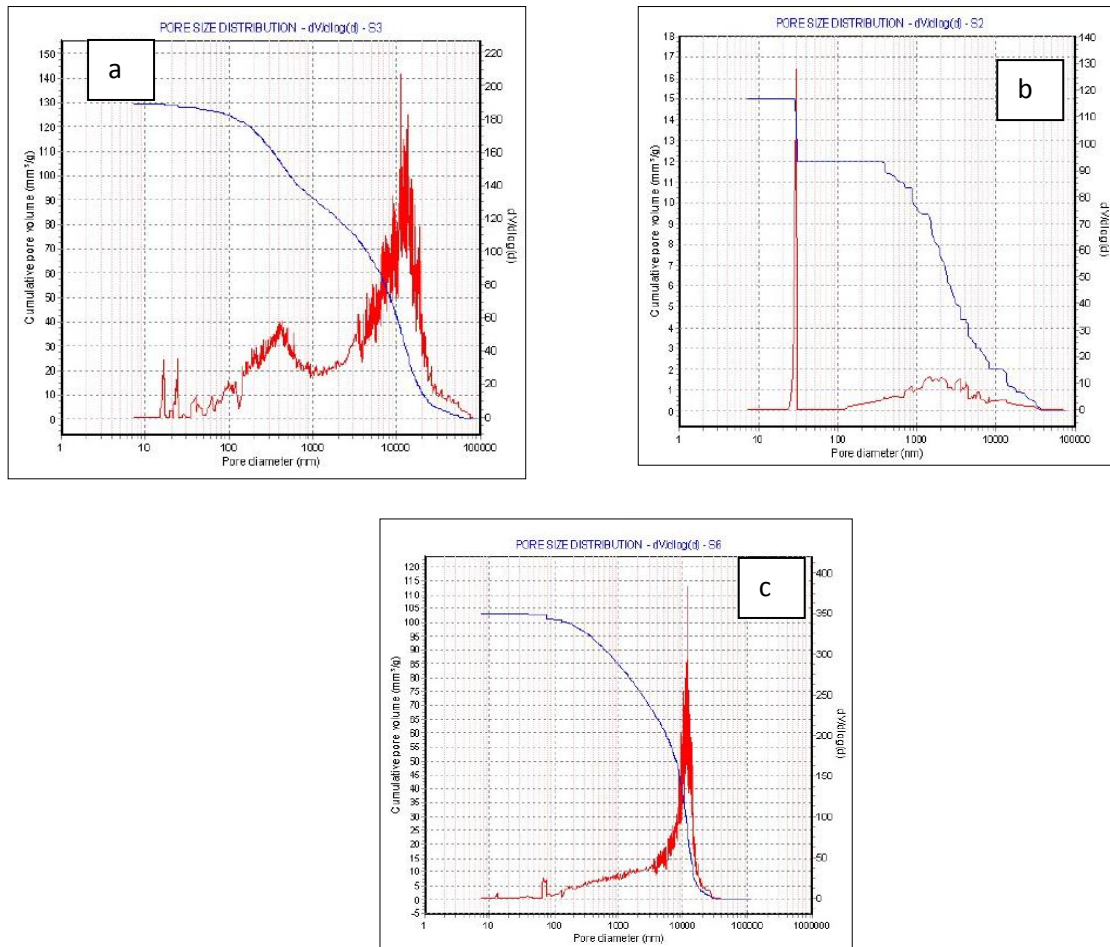


Figure 5. Pore size distribution and mercury capillary curves showing (a) bimodal pore size distribution in parallel laminated sandstone, (b) bimodal pore size distribution in bioturbated sandstone and (c) unimodal pore size distribution in massive fine grained sandstone.

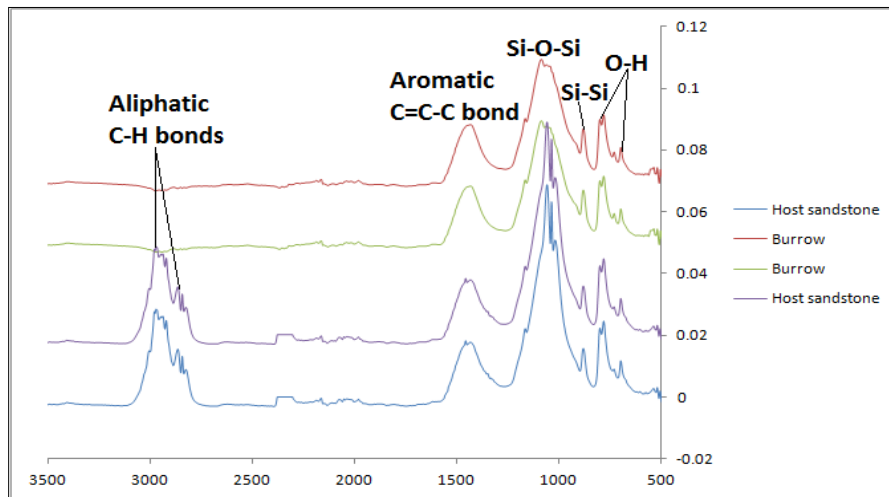


Figure 6. FTIR spectra of burrowed and non burrowed zones showing a dominance of aromatic functional groups in the burrows.

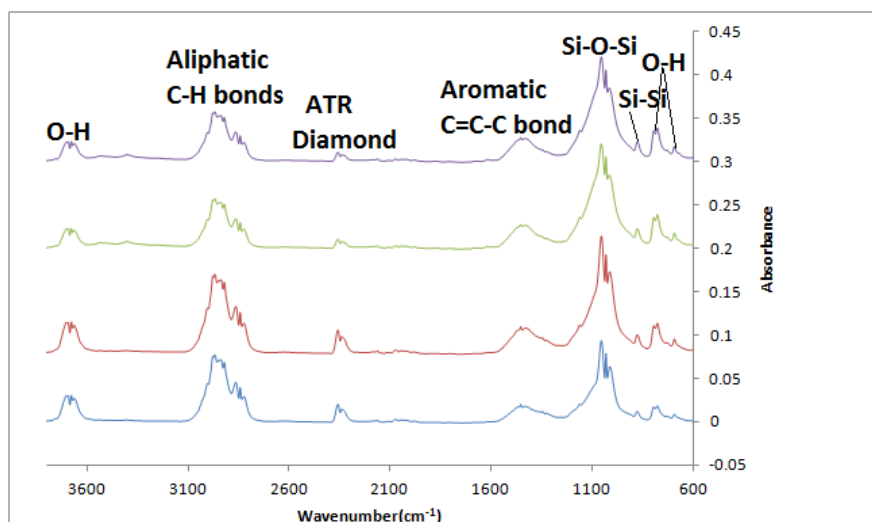


Figure 7. FTIR spectra of selected points in massive fine grained sandstones showing presence of both aliphatic and aromatic hydrocarbon functional groups.

4.4. Relationship between micropermeability and amount of hydrocarbon

The control of micro permeability on hydrocarbon distribution is evident in the samples with some form of heterogeneities. Such heterogeneities include structurally-induced heterogeneities in the laminated sandstones and texturally-induced heterogeneities in the bioturbated sandstones.

4.4.1. Parallel laminated sandstone

In the parallel laminated sandstones, permeability distribution in the samples is controlled mainly by the lamination type (Figures 8 and 9). The sand-dominated laminations recorded higher permeability values than the silt-dominated laminations. This is attributed to the higher amount of intergranular pores in the sand-dominated laminations compared to the silt-dominated laminations. The absorbance of the hydrocarbon functional groups vary with the lamination type in which it is found and therefore is also influenced by the permeability distribution in the samples. Statistical analysis of the relationship between hydrocarbon bond absorbance and micropermeability distribution shows a significant (Tables 2 and 3) negative relationship between the two parameters with Pearson correlation coefficient values of -0.90 and -0.97 in laminated sandstones 1 and 2 respectively. The sampled points with high permeability generally have lower absorbance of hydrocarbon functional groups and vice versa. The correlation coefficient (R^2) between hydrocarbon bond absorbance and micropermeability in laminated sandstones 1 and 2 is 0.81 and 0.95 respectively indicating a strong correlation [42] between bond absorbance and micropermeability.

Table 2. Pearson correlation between micropermeability (mD) and hydrocarbon bond absorbance

		Absorbance	Permeability
Absorbance	Pearson Correlation	1	-0.899**
	Sig. (2-tailed)		0.000
	N	21	21
Permeability	Pearson Correlation	-0.899**	1
	Sig. (2-tailed)	0.000	
	N	21	21

** . Correlation is significant at the 0.01 level (2-tailed)

Table 3. Pearson correlation between micropermeability (mD) and hydrocarbon bond absorbance

		Absorbance	Permeability
Absorbance	Pearson Correlation	1	-0.972**
	Sig. (2-tailed)		0.000
	N	64	64
Permeability	Pearson Correlation	-0.972**	1
	Sig. (2-tailed)	0.000	
	N	64	64

** . Correlation is significant at the 0.01 level (2-tailed)

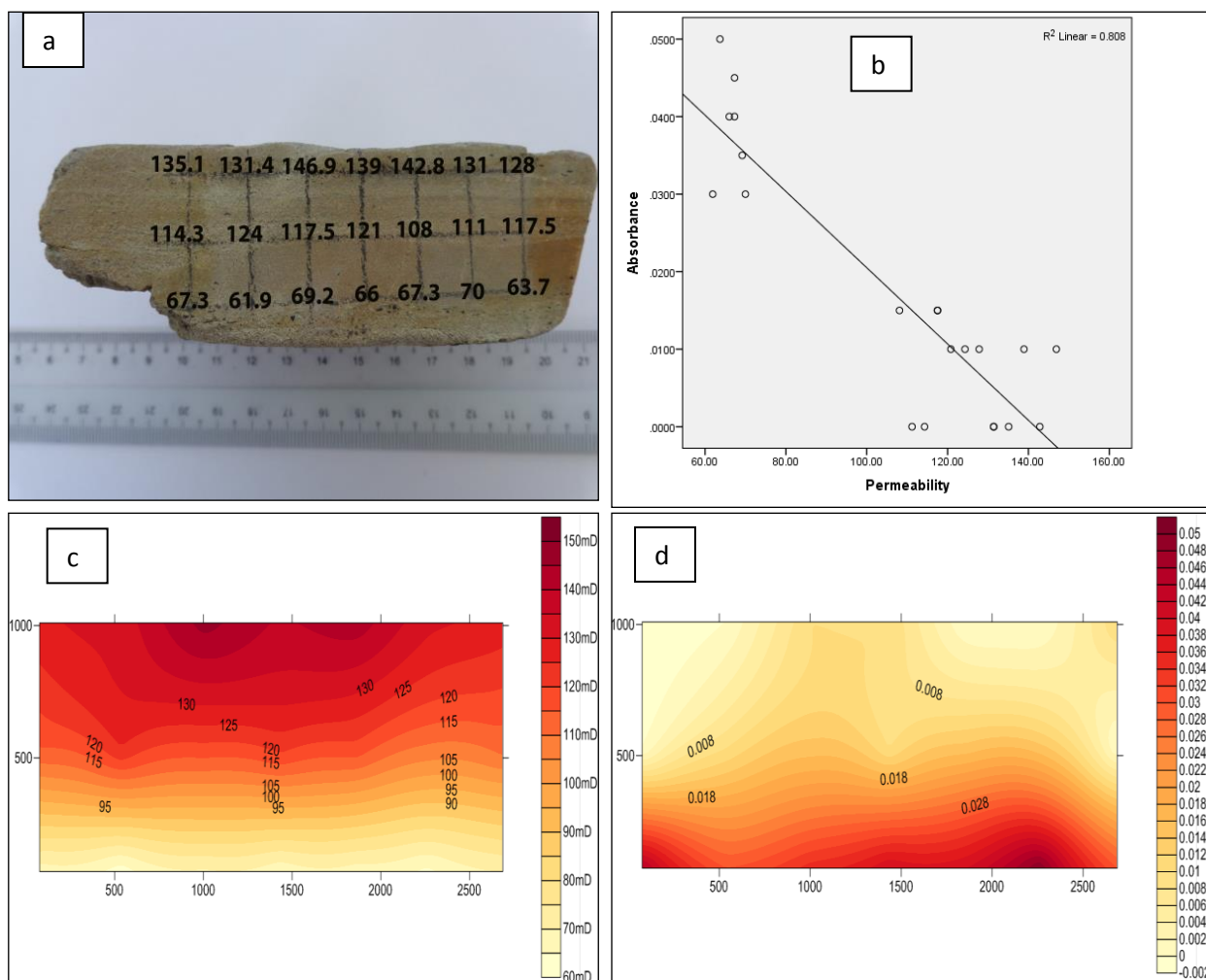


Figure 8. Laminated sandstone 1 showing (a) micropermeability distribution, (b) correlation between absorbance and micropermeability (R^2) = 0.81, c. pictorial representation of micropermeability and (d) pictorial representation of aromatic C=C-C stretching bond.

4.4.2. Massive fine grained sandstone

Permeability distribution in the massive fine-grained sandstones random and do not seem to follow any particular trend. A similar random pattern in the distribution of hydrocarbon functional groups is also observed in these samples. However a strong correlation between micropermeability and absorbance of hydrocarbon bonds still exists with coefficient of correlation values (R^2) of 0.79 and 0.91 in massive fine grained sandstone samples 1 and 2 respectively (Figures 10 and 11). Tables 4 and 5 show that the relationship between micropermeability and hydrocarbon bond absorbance in massive fine-grained sandstones is a

significant negative relationship with Pearson correlation coefficient of -0.89 and -0.95 in samples S1 and S2 respectively indicating a control of micropermeability on hydrocarbon distribution despite the randomness in the distribution.

Table 4. Pearson correlation between micropermeability (mD) and hydrocarbon bond absorbance

		Absorbance	Permeability
Absorbance	Pearson Correlation	1	-0.888**
	Sig. (2-tailed)		0.000
	N	32	32
Permeability	Pearson Correlation	-0.888**	1
	Sig. (2-tailed)	0.000	
	N	32	32

** Correlation is significant at the 0.01 level (2-tailed)

Table 5. Pearson correlation between micropermeability (mD) and hydrocarbon bond absorbance

		Absorbance	Permeability
Absorbance	Pearson Correlation	1	-0.954**
	Sig. (2-tailed)		0.000
	N	35	35
Permeability	Pearson Correlation	-0.954**	1
	Sig. (2-tailed)	0.000	
	N	35	35

** Correlation is significant at the 0.01 level (2-tailed)

4.4.3. Bioturbated sandstones

In the bioturbated sandstones, permeability values in the host sandstone are generally several orders of magnitude higher than permeability in the burrows (Figures 12 and 13). In terms of peak absorbance, the absorbance of the hydrocarbon peaks are much higher in the less permeable burrows compared to the more permeable host sandstones. This indicates an inverse relationship between micropermeability and absorbance of hydrocarbon functional groups. The relationship between micro permeability and peak absorbance is determined to be significant ($p \leq 0.01$) (Tables 6 and 7) with a correlation coefficient (R^2) of 0.71 and 0.71, and Pearson correlation coefficient of -0.79 and -0.84 respectively indicating a strong negative correlation between permeability and absorbance of hydrocarbon bonds.

Table 6. Pearson correlation between micropermeability (mD) and hydrocarbon bond absorbance

		Absorbance	Permeability
Absorbance	Pearson Correlation	1	-0.785**
	Sig. (2-tailed)		0.000
	N	60	60
Permeability	Pearson Correlation	-0.785**	1
	Sig. (2-tailed)	0.000	
	N	60	60

** Correlation is significant at the 0.01 level (2-tailed)

Table 7. Pearson correlation between micropermeability (mD) and hydrocarbon bond absorbance

		Absorbance	Permeability
Absorbance	Pearson Correlation	1	-0.844**
	Sig. (2-tailed)		0.000
	N	60	60
Permeability	Pearson Correlation	-0.844**	1
	Sig. (2-tailed)	0.000	
	N	60	60

** Correlation is significant at the 0.01 level (2-tailed)

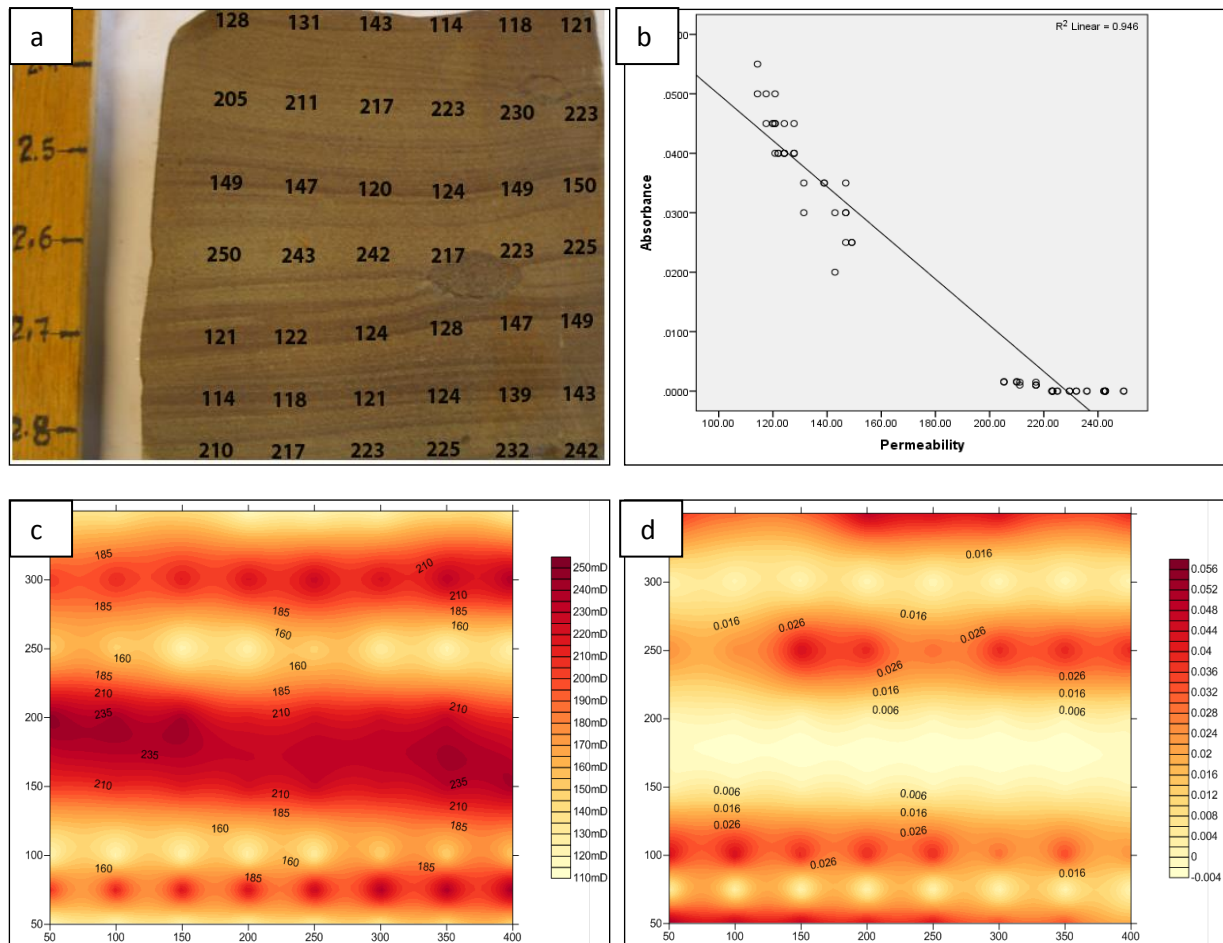


Figure 9. Laminated sandstone 2 showing (a) micropermeability distribution, (b) correlation between absorbance and micropermeability (R^2) = 0.95, (c) pictorial representation of micropermeability and (d) pictorial representation of aliphatic C-H.

5. Conclusion

FTIR analysis of the samples reveal the main hydrocarbon functional groups present to be aliphatic C-H stretching and aromatic C=C-C stretching bonds. The distribution of hydrocarbon bonds in the samples are controlled mainly by textural and structurally-induced heterogeneities in the samples such as the variable textural domains in the bioturbated sandstones with burrows and different lamination types in the laminated sandstones. In the laminated sandstones, there is a concentration of aromatic bonds in the silt-dominated laminations whereas in the bioturbated sandstones there is a concentration of aromatic bonds in the burrows. These heterogeneities also control the micropermeability and pore size distribution within these samples. In the massive fine-grained sandstones which lack any form of macro scale heterogeneities, distribution of hydrocarbon bonds and micropermeability is random. High permeability generally correlates with low absorbance of hydrocarbon functional groups and vice-versa. Correlation between micropermeability and hydrocarbon bond absorbance show a strong negative relationship between the two parameters. Statistical analysis indicate that the relationship is significant ($p \leq 0.01$).

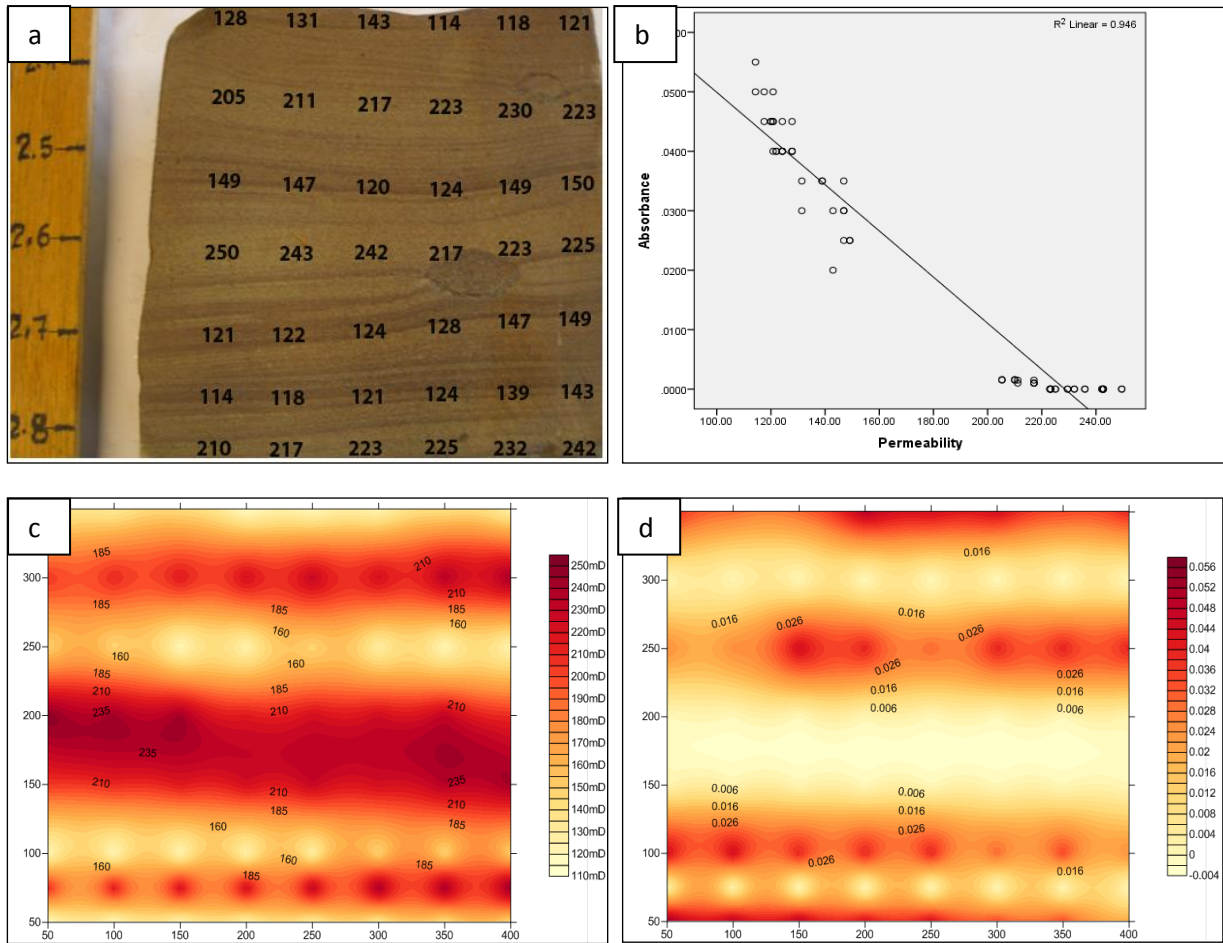
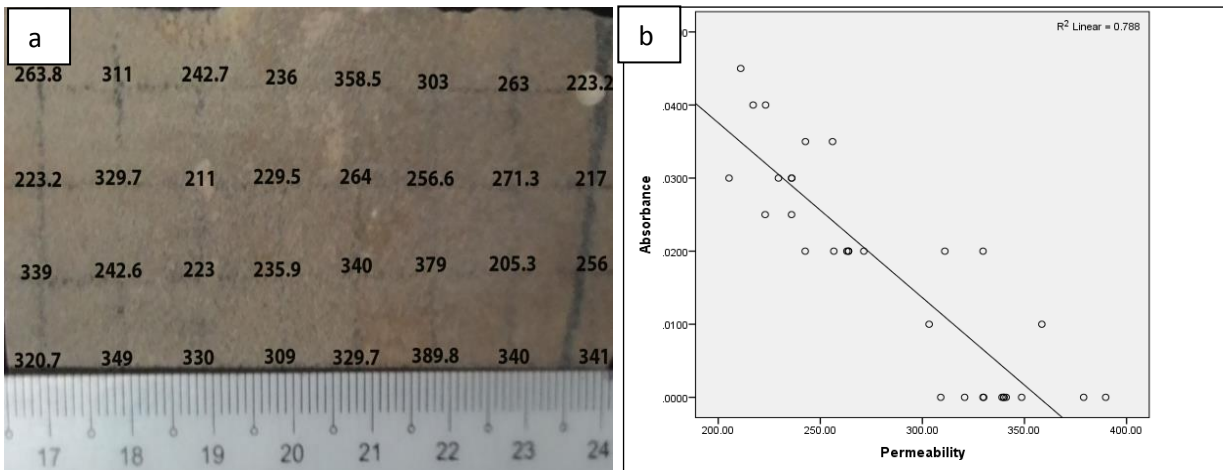


Figure 9. Laminated sandstone 2 showing (a) micropermeability distribution, (b) correlation between absorbance and micropermeability (R^2) = 0.95, (c) pictorial representation of micropermeability and (d) pictorial representation of aliphatic C-H.



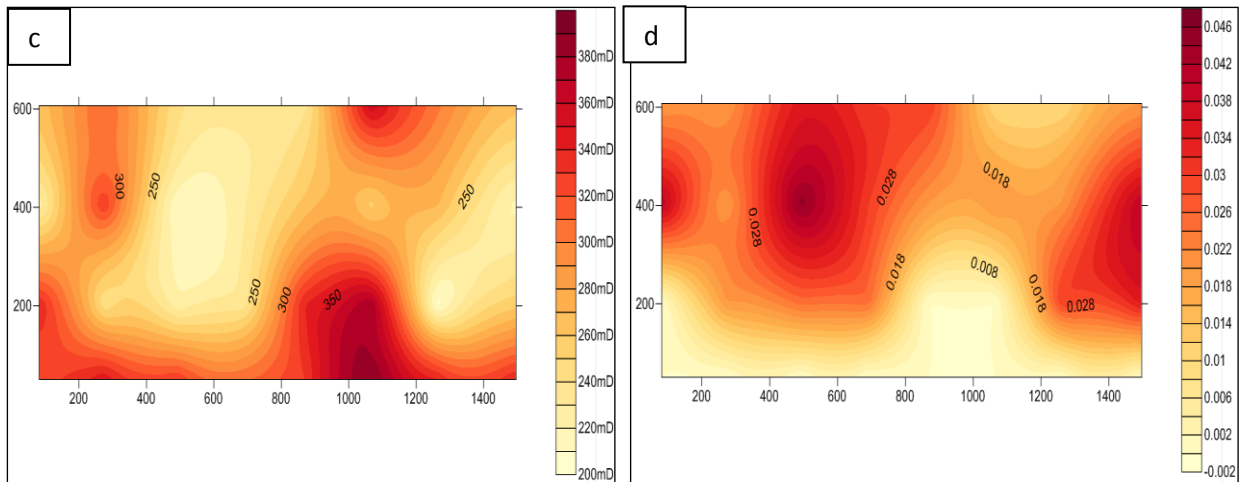


Figure 10. Massive fine-grained sandstone sample 1 showing (a) micropermeability distribution (b) correlation between absorbance and micropermeability ($R^2 = 0.79$), (c) pictorial representation of micropermeability and d. pictorial representation of aliphatic C-H bond.

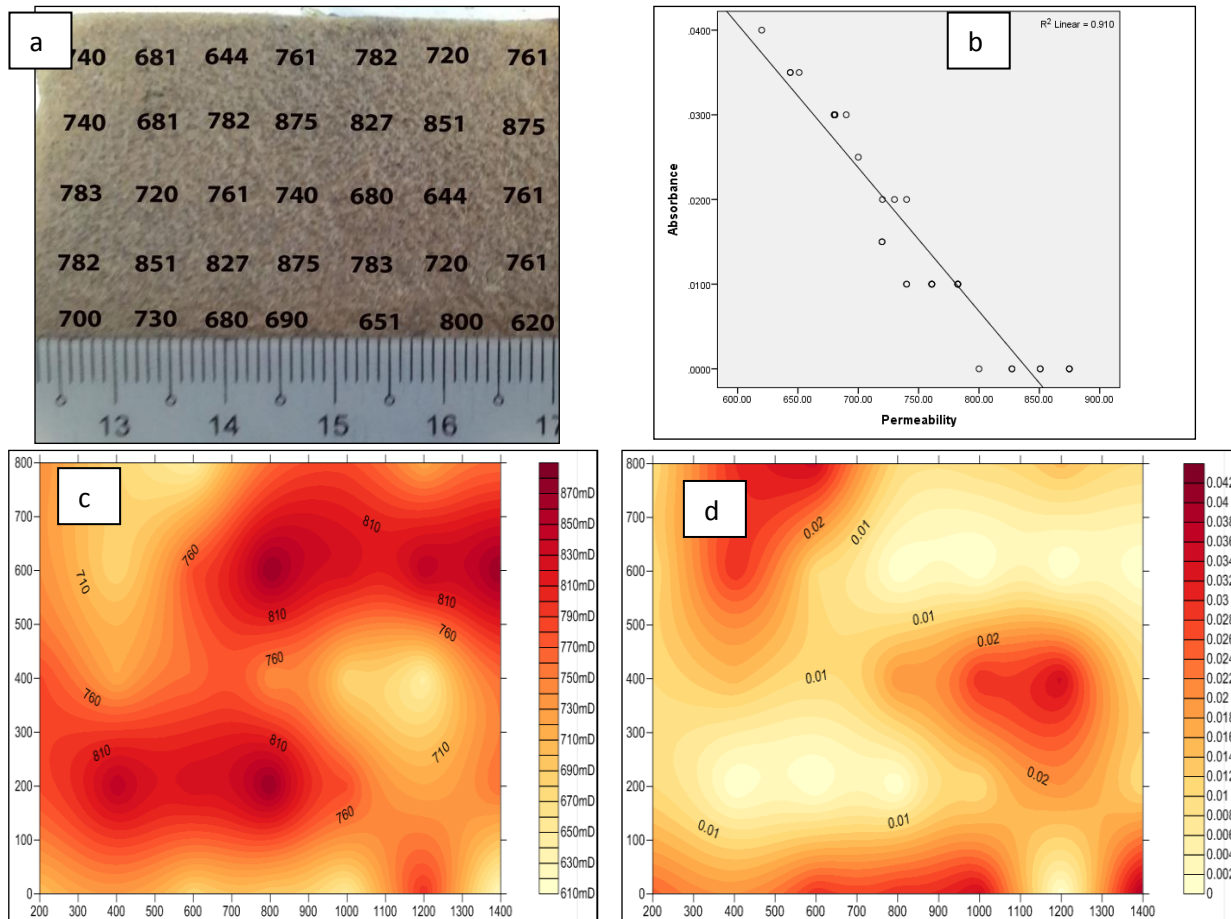


Figure 11. Massive fine-grained sandstone sample 2 showing (a) micropermeability distribution (b) correlation between absorbance and micropermeability ($R^2 = 0.91$), c. pictorial representation of micropermeability and (d) pictorial representation of aliphatic C-H stretching bond.

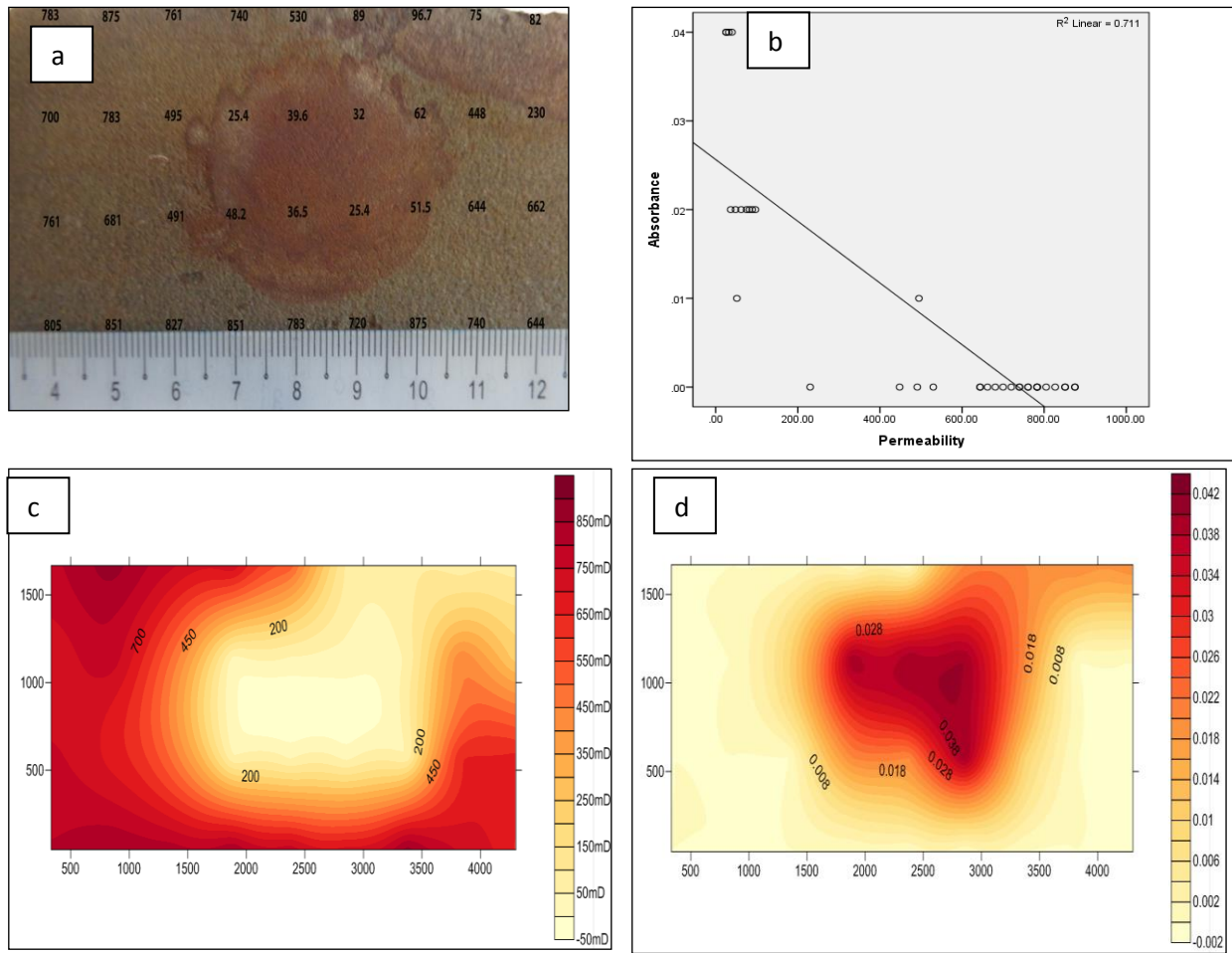
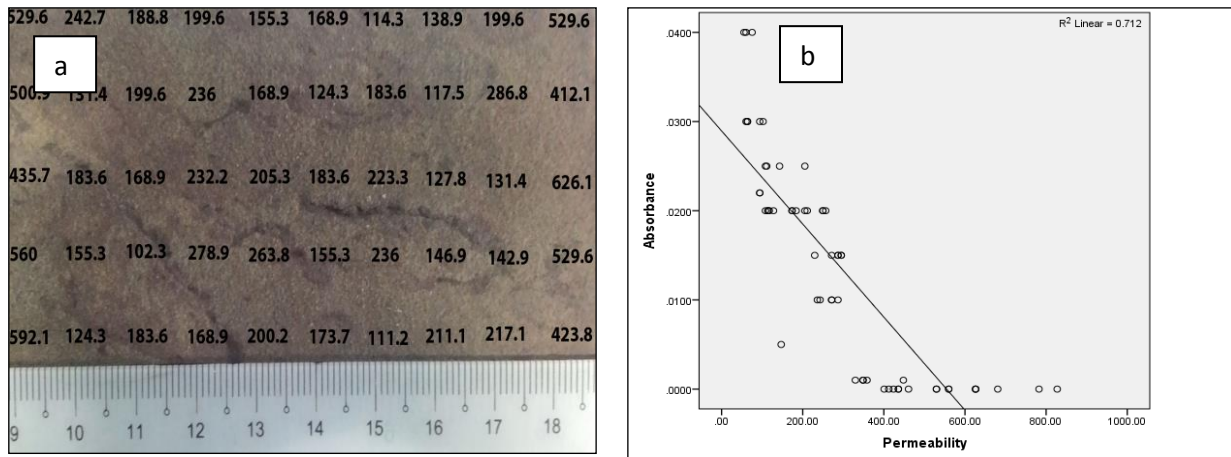


Figure 12. Bioturbated sandstone 1 showing (a) micropermeability distribution, (b) correlation between absorbance and micropermeability ($R^2 = 0.71$), (c) pictorial representation of micropermeability and (d) pictorial representation of aromatic C=C-C stretching bond.



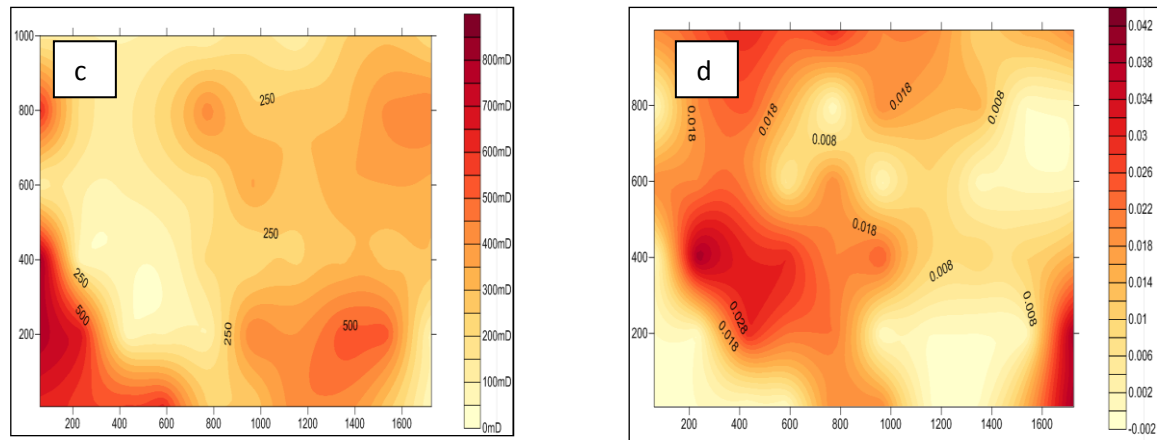


Figure 13. Bioturbated sandstone 2 showing (a) micropermeability distribution, (b) correlation between absorbance and micropermeability (R^2) = 0.71, c. pictorial representation of micropermeability and (d) pictorial representation of aromatic C=C-C stretching bond.

References

- [1] Kocberber R, and Colling R. 1990, Impact of reservoir heterogeneity on initial distribution of hydrocarbons. Proceedings of SPE Annual Technical Conference and Exhibition, New Orleans.
- [2] Davis RA Jr, 1983. Depositional systems, Prentice-Hall Inc., Englewood Cliffs, New Jersey.
- [3] Galloway WE, and Hobday DK. 1983, Terrigenous clastic depositional systems, Springer-Verlag Inc., New York.
- [4] Reineck HE, and Singh IB. 1975, Depositional sedimentary environments, Springer Berlin, 437p.
- [5] Selley R. 1996 Ancient sedimentary environments and their sub-surface diagnosis. Chapman and Hall, London, 300p.
- [6] Tucker ME. 2003, Sedimentary rocks in the field. John Wiley & Sons, 234p.
- [7] Moraes MA, and Surdam RC. 1993, Diagenetic heterogeneity and reservoir quality; Fluvial, deltaic, and turbiditic sandstone reservoirs, Potiguar and Reconcavo Rift Basins, Brazil. American Association of Petroleum Geologists Bulletin, 77, 1142-1158.
- [8] Morad S, Al-Ramadan K, Ketzer JM, and De Ros LF. 2010, The impact of diagenesis on the heterogeneity of sandstone reservoirs: A review of the role of depositional facies and sequence stratigraphy. AAPG Bulletin, 94, 1267-1309.
- [9] Tonkin NS, McIlroy D, Meyer R, and Moore-Turpin A. 2010, Bioturbation influence on reservoir quality: A case study from the Cretaceous Ben Nevis Formation, Jeanne d'Arc Basin, offshore Newfoundland, Canada. AAPG Bulletin, 94, 1059-1078.
- [10] Pryor WA. 1973, Permeability-porosity patterns and variations in some Holocene sand bodies. American Association of Petroleum Geologists Bulletin, 57, 162-189.
- [11] Weber KJ. 1982, Influence of common sedimentary structures on fluid flow in reservoir models. Journal of Petroleum Technology, 34, 665-672.
- [12] Roller CB, Driskill B, and Manrique JF. 2009, Use of the Allan variance for characterizing reservoir heterogeneity. Society of Petrophysicists and Well Log Analysts (SPWLA) 50TH Annual Logging Symposium, Woodlands, Texas, USA., 1-10.
- [13] Rashid B, Muggeridge AH, Bal A, and Williams G. 2012, Quantifying the impact of permeability heterogeneity on secondary-recovery performance. Society of Petroleum Engineers (SPE) Journal, 6, 455-468.
- [14] Pan C, Feng J, Tian Y, and Yu L. 2005, Interaction of oil components and clay minerals in reservoir sandstones. Organic Geochemistry, 36, 633-654.

- [15] Pan C, and Yang J. 2000, Geochemical characteristics and implications of hydrocarbons in reservoir rocks of Junggar Basin, China. *Chemical Geology*, 167, 321–335.
- [16] Maciel GE, Bartuska VJ, and Miknis FP. 1978, Correlation between oil yields of oil shale and ¹³C nuclear magnetic resonance spectra. *Fuel*, 57, 505–506.
- [17] Solomon PR, and Miknis FP. 1980, Use of Fourier transform infrared spectroscopy for determining oil shale properties. *Fuel*, 59, 893–896.
- [18] Miknis FP. 1992, Combined NMR and Fischer assay study of oil shale conversion. *Fuel*, 71, 731–738.
- [19] Evdokimov IN, and Losev AP. 2007, Potential of UV-visible absorption spectroscopy for characterizing crude petroleum oils. *Oil and Gas Business*, 1–21.
- [20] Washburn KE, and Birdwell JE. 2013, Multivariate analysis of ATR-FTIR spectra for assessment of oil shale organic geochemical properties. *Organic Geochemistry*, 63, 1–7.
- [21] Coates J. 2000, Interpretation of Infrared Spectra, A Practical Approach Interpretation of Infrared Spectra, A Practical Approach. In *Encyclopedia of Analytical Chemistry*. John Wiley and Sons.
- [22] Stuart, B. (2005). *Infrared Spectroscopy: Fundamentals and Applications*, Wiley, 203p.
- [23] Smith GH. 1996, *Organic Chemistry*. St. Louis: Mosby-Year Book, Inc, 1208p.
- [24] Hutchinson C. 2005, *Geology of North West Borneo: Sarawak, Brunei and Sabah*, Elsevier, New York, 421pp.
- [25] Tan DNK, Rahman AHB, Anuar A, Bait B, & Tho CK. (1999). West Baram Delta. In L. K. Meng (Ed.), *The Petroleum Geology and Resources of Malaysia*. Petroleam Nasional Berhad (PETRONAS), Kuala Lumpur, pp. 291-341.
- [26] Ho KF. 1978, Stratigraphic framework for oil exploration in Sarawak. *Bulletin of the Geological Society of Malaysia*, 10, 1–13.
- [27] Rijks EJJ. 1981, Baram Delta geology and hydrocarbon occurrence (Sarawak). *Geological Society of Malaysia Bulletin*, 14, 1–8.
- [28] Abd. Rahman AH, Menier D, and Mansor, MY. 2014, Sequence stratigraphic modelling and reservoir architecture of the shallow marine successions of Baram field, West Baram Delta, offshore Sarawak, East Malaysia. *Marine and Petroleum Geology*, 58, pp.687–703.
- [29] Madon M. 1999, Geological setting of Sarawak. In: Meng, LK (Ed.), *The Petroleum Geology and Resources of Malaysia*. Petroleam Nasional Berhad (PETRONAS), Kuala Lumpur, 273-290.
- [30] Madon M, Kim CL, and Wong R. 2013, The structure and stratigraphy of deepwater Sarawak, Malaysia: Implications for tectonic evolution. *Journal of Asian Earth Sciences*, 76, 312–333.
- [31] Cullen A, 2014. Nature and significance of the West Baram and Tinjar Lines, NW Borneo. *Marine and Petroleum Geology*, 51, 197–209.
- [32] Johnson HD, Kuud T, and Dundang A. 1989, Sedimentology and reservoir geology of the Betty Field, Baram Delta Province, offshore Sarawak, NW Borneo. *Bulletin of the Geological Society of Malaysia*, 25, 119–161.
- [33] Pettijohn FJ, Potter PE, and Siever R. 1987, *Sand and Sandstones*, 611p.
- [34] Boggs SJ. 2009, *Petrology of sedimentary rocks*, Cambridge University Press, London, 600pp.
- [35] Giesche H. 2006, Mercury porosimetry: a general (practical) overview. *Particle and Particle Systems Characterization*, 23, 1–11.
- [36] Miller J. 1988, Microscopical Technique: I. Slices, Slides, Stains and Peels. In M. E. Tucker (Ed.), *Techniques in Sedimentology*, Durham, 86-107.
- [37] Taylor AM, and Goldring R. 1993, Description and analysis of bioturbation and ichnofabric. *Journal of Geological Society of London*, 150, 141–148.

- [38] Ben-Awuah J, Padmanabhan E, Andriamihaja S, Ofori Amponsah P, and Ibrahim, Y. 2016, Petrophysical and reservoir characteristics of sedimentary rocks from offshore West Baram Delta, Sarawak Basin, Malaysia. *Pet Coal*, 58(4), 414-429.
- [39] Ben-Awuah J, and Padmanabhan E. 2015, Effect of bioturbation on reservoir rock quality of sandstones: A case study from the Baram Delta, offshore Sarawak, Malaysia. *Journal of Petroleum Exploration and Development*, 42, 1-9.
- [40] Ben-Awuah J, and Padmanabhan E. 2014, Impact of bioturbation on reservoir quality: A case study of biogenically reduced permeabilities of reservoir sandstones of the Baram Delta, Sarawak, Malaysia. *Journal of Applied Sciences*, 14, 3312-3317.
- [41] Silverstein RM, Webster FX, and Kiemle DJ. 2005, Spectrometric identification of organic compounds. John Wiley & Sons, New York, 502p.
- [42] Rumsey DJ. 2011, Statistics for Dummies. For Dummies, Ohio, 384p.
- [43] Ryan WBF, Carbotte SM, Coplan JO, O'Hara S, Melkonian A, Arko R, Zemsky R. 2009, Global multi-resolution topography synthesis. *Geochemistry Geophysics Geosystems*, 10(3).

*Corresponding author: jbenawuah@gmail.com / benawuah@ucsiuniversity.edu.my